Inorganic Chemistry

Article

pubs.acs.org/IC

Encapsulation of a Metal Complex within a Self-Assembled Nanocage: Synergy Effects, Molecular Structures, and Density Functional Theory Calculations

Christophe Desmarets,*[,†,‡] Geoffrey Gontard,[†,‡] Andrew L. Cooksy,[§] Marie Noelle Rager,[⊥] and Hani Amouri*[,†,‡]

[†]Institut Parisien de Chimie Moléculaire (IPCM), UMR 8232, Sorbonne Universités, Université Paris 06, Université Pierre et Marie Curie (UPMC), 4 place Jussieu, 75252 Paris Cedex 05, France

[‡]IPCM, UMR 8232, Centre National de la Recherche Scientifique (CNRS), 4 place Jussieu, 75252 Paris Cedex 05, France

[§]Department of Chemistry and Biochemistry, San Diego State University, 5500 Campanile Drive, San Diego California 92182-1030, United States

[⊥]Institut de Recherche de Chimie Paris, CNRS−Chimie ParisTech, 11 rue Pierre et Marie Curie, 75005 Paris, France

Supporting Information

ABSTRACT: A novel palladium-based metallacage was self-assembled. This nanocage displayed two complementary effects that operate in synergy for guest encapsulation. Indeed, a metal complex, $[Pt(NO_2)_4]^{2-}$, was hosted inside the cavity, as demonstrated by solution NMR studies. Single-crystal X-ray diffraction shows that the guest adopts two different orientations, depending on the nature of the host−guest interactions involved. A density functional theory computational study is included to rationalize this type of host−guest interaction. These studies pave the way to a better comprehension of chemical interaction and transformation within confined nanospaces.

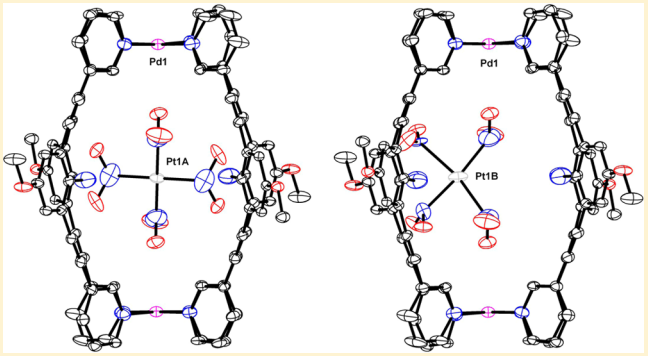

INTRODUCTION

The rational design of inorganic artificial receptors for host−guest chemistry is one of the most attractive areas in contemporary supramolecular chemistry.[1] Self-assembly is now well-established as an elegant "bottom-up" method for fabricating elaborate architectures[2] such as helicates,[3] cages,[4] metallacryptands,[5] metallacycles,[6] and coordination polymers.[7] This approach becomes particularly powerful when the ease of control offered by the self-assembly of organic components is combined with the electronic, ion-sensing, catalytic, magnetic, or photonic properties of inorganic components. In the past decade, there has been intensive research in the preparation of metallacages, which have shown particular promise in the chemistry of host−guest interactions.[8]

Research activities in our group have been focused on the assembly of cagelike systems that incorporate a central cavity where anions can be encapsulated. Thus, we have developed syntheses of some metallacryptands and discrete 3D capsules that are able to encapsulate weakly coordinated anions.[5a,9] For instance, our metallacages of the type M_2L_4 [M = Co; L = bis(benzimidazole)-1,3-phenylene] were perfectly designed to house BF_4 anions, where the encapsulated anion interacts with the two cobalt centers through M−F contacts.

Pursuing our research in this area, we sought other types of templating guests, notably organometallic complexes. Prior to this work, only a few examples of inorganic receptors capable of encapsulating a metal complex had been reported: for example, a coordination box encapsulating discrete stacks of square-planar complexes, described by Fujita et al.[10] Therrien et al constructed a large cationic hexanuclear metallaprism capable of hosting a square-planar metal complex.[11] A coordination cage encapsulating a stacked platinum complex of the Magnus salt type has been reported by the group of Clever, Shionoya, and co-workers.[12] Furthermore, a dinuclear palladium molecular complex that encapsulates two *cis*-platin molecules inside the metallosupramolecular cavity was reported by Crowley et al.[13]

Herein, we report a rational, high-yield (>90%) strategy for the preparation of nanocages (Figure 1) based on palladium coordination chemistry, and we demonstrate their properties as metal complex hosts. These novel nanocages incorporate unsaturated palladium centers—which may act as electrostatic anchors—and bridging ligands containing endohedral amino

Received: October 8, 2013
Published: April 11, 2014

dx.doi.org/10.1021/ic402539x | *Inorg. Chem.* 2014, 53, 4287−4294

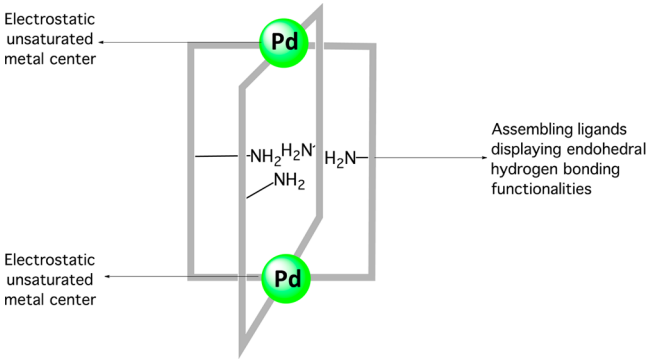

Figure 1. Schematic drawing of the Pd_2L_4 nanocage displaying both functionalities that operate in synergy for guest encapsulation.

functionality for hydrogen bonding. Both effects operate in a synergistic manner to enhance host–guest interactions.

EXPERIMENTAL SECTION

General Information and Materials. All solvents used were reagent grade or better. Commercially available reagents were used as received. 2,6-Dibromo-4-methoxyaniline[14] and $[Pd(CH_3CN)_4][OTf]_2$[15] were prepared according to published methods. All experimental manipulations were carried out under argon using Schlenk techniques. IR spectra were recorded on a Bruker Tensor 27 spectrometer equipped with a Harrick ATR instrument. Elemental analyses were performed by the microanalytical laboratory of ICSN, Gif-sur Yvette, France. Positive-mode electrospray ionization mass spectrometry (ESI-MS) spectra were obtained using a triple-quadrupole mass spectrometer (Quattro I Micromass). Automatic data acquisition was processed using the software *Masslynx 3.4*. NMR experiments were carried out on a Bruker Avance II 300 MHz or a Bruker Avance III HD 400 MHz spectrometer operating at 297 K with chemical shifts referenced to residual solvent peaks. Chemical shifts are reported in parts per million (ppm) and coupling constants (J) in hertz (Hz). Standard abbreviations indicating the multiplicity were used as follows: m = multiplet, t = triplet, d = doublet, s = singlet, and b = broad.

Synthesis of 2,6-Diethynyl-4-methoxyaniline (1). A Schlenk flask was charged with 2,6-dibromo-4-methoxyaniline (1 g, 3.55 mmol), CuI (67 mg, 0.355 mmol), and $[Pd(PPh_3)_4]$ (410 mg, 0.355 mmol). The Schlenk flask was vacuum-purged and refilled with argon (three times). Distilled tetrahydrofuran (THF; 7 mL) and Et_3N (7 mL) were introduced. Then trimethylsilylacetylene (5.05 mL, 35.5 mmol) was added. The reaction mixture was then heated to 60 °C and allowed to stir for 48 h. After cooling, solvents were removed under vacuum, and the crude product was first purified by column chromatography (hexane/AcOEt = 90/10) to afford a yellow oil. A KOH/MeOH solution was then prepared (1 g into 25 mL) and added to the crude mixture previously obtained. The solution was then stirred overnight. The solvent was removed by reduced pressure, and the product was purified via column chromatography (hexane/AcOEt = 70/30): 590 mg of yellow solid (97%). IR (ATR; ν, cm^{-1}): 3433 (NH_2), 3328 (C≡C–H), 3265, 3004, 2947, 2829, 2094 (C≡C), 1682, 1620, 1593 (N–H), 1460, 1431, 1325, 1290, 1264, 1230, 1188, 1140, 1051, 936, 873, 840, 609, 472, 349, 235. ^{1}H NMR (300 MHz, CD_2Cl_2): δ 6.95 (s, 2H, H_b), 4.60 (bs, 2H, NH_2), 3.74 (s, 3H, OMe), 3.50 (s, 2H, H_f). ^{13}C NMR (75 MHz, CD_3CN): δ 150.9 (C_a), 145.5 (C_d), 119.6 (C_b), 107.4 (C_c), 83.2 (C_e), 80.1 (C_f), 56.3 (COMe). ESI-MS. Calcd for $[1H]^+$: m/z 172.07. Found: m/z 172.2. Anal. Calcd for $C_{11}H_9NO$: C, 77.17; H, 5.30; N, 8.18. Found: C, 76.89; H, 5.33; N, 7.97.

Synthesis of 2,6-(3-Pyridylethynyl)-4-methoxyaniline (2). A Schlenk flask was charged with **1** (500 mg, 2.9 mmol), CuI (55 mg, 0.29 mmol), $[Pd(PPh_3)_4]$ (337 mg, 0.29 mmol), and 3-bromopyridine (0.7 mL, 0.725 mmol). The Schlenk flask was vacuum-purged and refilled with argon (three times). Distilled THF (8 mL) and Et_3N (8 mL) were introduced. The reaction mixture was then heated to 60 °C and allowed to stir for 48 h. After cooling, solvents were removed under vacuum, and the crude product was purified by column chromatography with AcOEt (100%): 710 mg of yellow solid (75%). IR (ATR; ν, cm^{-1}): 3452 (NH_2), 3367, 2932, 2838, 2200 (C≡C), 1730, 1572 (N–H), 1643, 1435, 1403, 1361, 1309, 1273, 1231, 1214, 1182, 1127, 1044, 1020, 940, 855, 837, 793, 696, 626, 582, 539, 491, 445, 396, 286, 212. ^{1}H NMR (300 MHz, CD_3CN): δ 8.81 (s, 2H, H_k), 8.58 (d, J = 4.9 Hz, 2H, H_j), 7.94 (d, J = 7.9 Hz, 2H, H_h), 7.42 (dd, J = 7.9 and 4.9 Hz, 2H, H_i), 7.06 (s, 2H, H_b), 4.99 (bs, 2H, NH_2), 3.77 (s, 3H, OMe). ^{13}C NMR (75 MHz, CD_3CN): δ 151.5 (C_k), 150.3 (C_j), 148.6 (C_a), 144.3 (C_d), 137.9 (C_b), 123.0 (C_i), 119.6 (C_g), 118.6 (C_b), 107.0 (C_c), 91.1 (C_e), 88.0 (C_f), 55.2 (COMe). ESI-MS. Calcd for $[2H]^+$: m/z 326.12. Found: m/z 326.13. Anal. Calcd for $C_{21}H_{15}N_6O$: C, 77.52; H, 4.65; N, 12.91. Found: C, 76.21; H, 4.84; N, 12.07.

Synthesis of [OTf⊂Pd_2(2)$_4$][OTf]$_3$ ([3][OTf]$_3$). Ligand **2** (100 mg, 0.30 mmol) was added to a solution of $[Pd(CH_3CN)_4][OTf]_2$ (87 mg, 0.15 mmol) in CH_3CN (15 mL). The yellow solution was stirred at room temperature 30 min, during which time the initially yellow solution turns to orange. The solvent was removed under vacuum. Hexane (10 mL) was then added. The solids were collected by filtration from the *n*-hexane solution, washed with CH_2Cl_2 (5 mL) and diethyl ether (3 × 5 mL), and dried under vacuum: 147 mg of orange solid (93%). This supramolecular cage was recrystallized from CH_3CN/Et_2O to afford quantitatively yellow crystals and was characterized as [**3**][OTf]$_3$. IR (ATR; ν, cm^{-1}): 3367 (NH_2), 3078, 2205 (C≡C), 1590 (N–H), 1465, 1439, 1417, 1364, 1236 (OTf), 1218, 1155, 1131, 1025, 946, 855, 809, 758, 693, 634, 573, 548, 515, 396, 354, 319. ^{1}H NMR (400 MHz, DMSO-d_6): δ 9.46 (d, J = 5.8 Hz, 8H, H_j), 9.23 (s, 8H, H_k), 8.26 (d, J = 8.0 Hz, 8H, H_h), 7.86 (dd, J = 8.0 and 5.8 Hz, 8H, H_i), 7.07 (s, 8H, H_b), 5.78 (bs, 8H, NH_2), 3.67 (s, 12H, OMe). ^{13}C NMR (100 MHz, DMSO-d_6): δ 152.8 (C_k), 150.2 (C_j), 150.1 (C_a), 145.7 (C_d), 142.6 (C_h), 127.6 (C_i), 123.1 (C_g), 119.9 (C_b), 106.2 (C_c), 92.7 (C_e), 90.2 (C_f), 55.8 (COMe). ESI-MS. Calcd for $[Pd_2(L^2)_4]^{4+}$: m/z 378.07. Found: m/z 378.5. Calcd for $[Pd_2(L^2)_4(CF_3SO_3)]^{3+}$: m/z 553.75. Found: m/z 554.7. Calcd for $[Pd_2(L^2)_4(CF_3SO_3)_2]^{2+}$: m/z 905.10. Found: m/z 906.3. Calcd for $[Pd_2(L^2)_4(CF_3SO_3)_3]^{+}$: m/z 1961.12. Found: m/z 1961.10. Anal. Calcd for $[C_{88}H_{60}F_{12}N_{12}O_{16}Pd_2S_4].4H_2O$: C, 48.43; H, 3.14; N, 7.70. Found: C, 47.97; H, 3.21; N, 7.30.

Synthesis of [[Pt(NO$_2$)$_4$]⊂Pd_2(2)$_4$][OTf]$_2$ ([4][OTf]$_2$). $K_2Pt(NO_2)_4$ (32 mg, 0.07 mmol) was added to a solution of [**3**][OTf]$_3$ (147 mg, 0.07 mmol) in CH_3CN (5 mL). The solution was stirred at room temperature for 30 min, during which time an orange precipitate formed. The solids were collected by filtration, washed with diethyl ether (3 × 5 mL), and dried under vacuum: 142 mg of orange solid (93%). This supramolecular cage was recrystallized from low diffusion of Et_2O to a CH_3CN/*N*,*N*-dimethylformaimde (DMF) solution, affording quantitatively yellow crystals, and was characterized as [**4**][OTf]$_2$. IR (ATR; ν, cm^{-1}): 3352 (NH_2), 3074, 2201 (C≡C), 2140, 1590 (N–H), 1565, 1464, 1404, 1331 (NO_2), 1311 (NO_2), 1279, 1235 (OTf), 1218, 1161, 1130, 1027, 946, 855, 807, 741, 696, 636, 585, 549, 516, 420, 398, 344, 313, 295. ^{1}H NMR (400 MHz, DMSO-d_6): δ 9.32 (d, J = 5.9 Hz, 8H, H_j), 9.22 (s, 8H, H_k), 8.22 (d, J = 8.1 Hz, 8H, H_h), 7.80 (dd, J = 8.1 and 5.9 Hz, 8H, H_i), 7.08 (s, 8H, H_b), 6.22 (bs, 8H, NH_2), 3.69 (s, 12H, OMe) ^{13}C NMR (100 MHz, DMSO-d_6): δ 151.9 (C_k), 150.1 (C_j), 149.9 (C_a), 146.0 (C_d), 142.5 (C_h), 127.6 (C_i), 123.0 (C_g), 119.9 (C_b), 105.7 (C_c), 91.9 (C_e), 89.8 (C_f), 55.9 (COMe). ESI-MS. Calcd for $[[Pt(NO_2)_4]\subset Pd_2(2)_4]^{4+}$: m/z) 946.61. Found: m/z 946.12. Anal. Calcd for $[C_{88}H_{60}F_{12}N_{12}O_{16}Pd_2S_4]\cdot 2H_2O$: C, 46.35; H, 2.90; N, 10.06. Found: C, 44.63; H, 2.72; N, 10.18.

X-ray Crystal Structure Determination of Metallacages [3][OTf]$_3$ and [4][OTf]$_2$. Data were collected on a Bruker Kappa APEXII. Determinations of the unit-cell parameters, data collection strategy, and integration were carried out with the Bruker *APEX2* suite of programs. A multiscan absorption correction was applied.[16] The structures were solved using *SIR92*[17] (**3**) and *SUPERFLIP*[18] (**4**) and refined anisotropically by full-matrix least-squares methods using *SHELXL-2013*.[19] Crystallographic data (excluding structure factors)

dx.doi.org/10.1021/ic402539x | *Inorg. Chem.* 2014, 53, 4287–4294

Scheme 1. Preparation of the Assembling Ligand 2

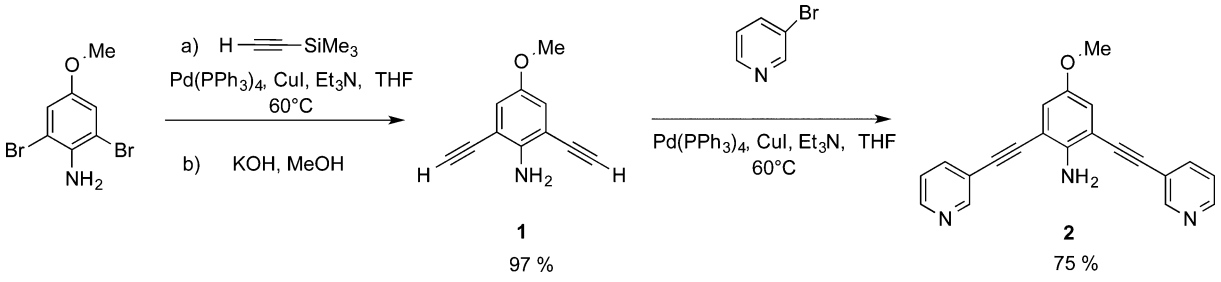

Scheme 2. Synthesis of the Palladium-Based Metallacage $[3][OTf]_3$

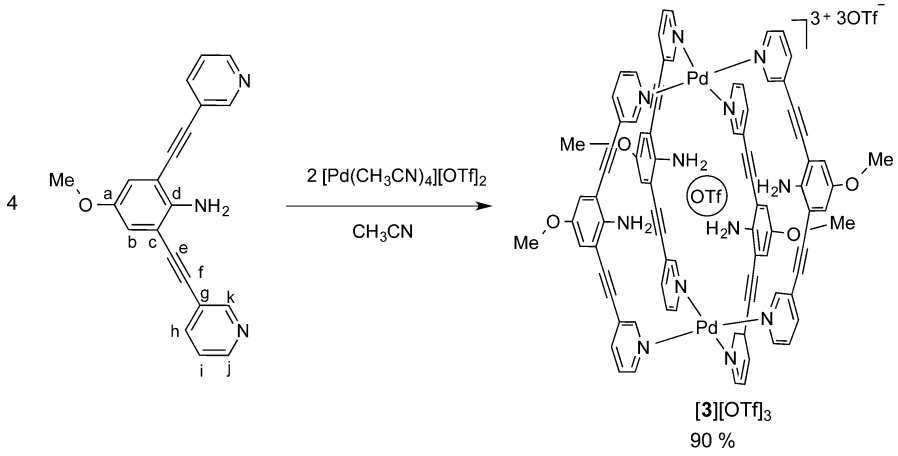

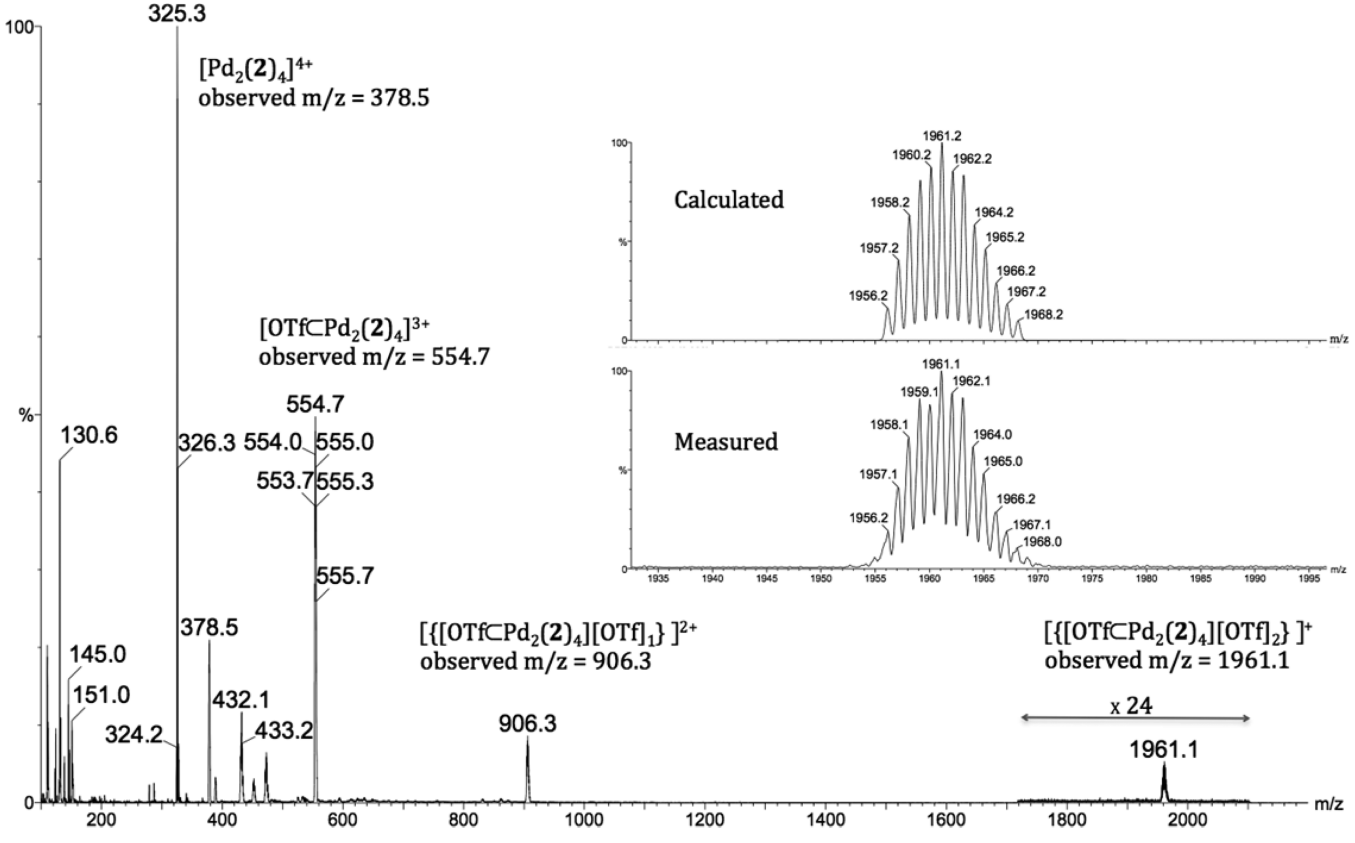

Figure 2. Partial ESI-MS spectrum illustrating the sequence of peaks corresponding to the intact metallacage $[3][OTf]_3$ associated with different numbers of triflate anions. Experimental and theoretical isotope distributions of $[\{[OTf⊂Pd_2(2)_4][OTf]_2\}]^+$.

dx.doi.org/10.1021/ic402539x | Inorg. Chem. 2014, 53, 4287−4294

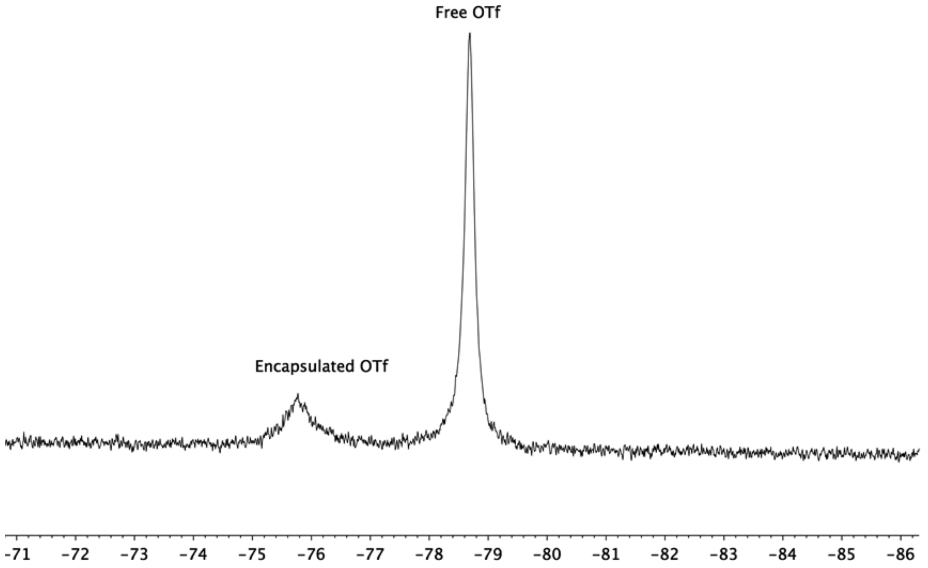

Figure 3. ^{19}F NMR spectrum of the metallacage [**3**][OTf]$_3$ recorded in acetone-d_6 at 25 °C.

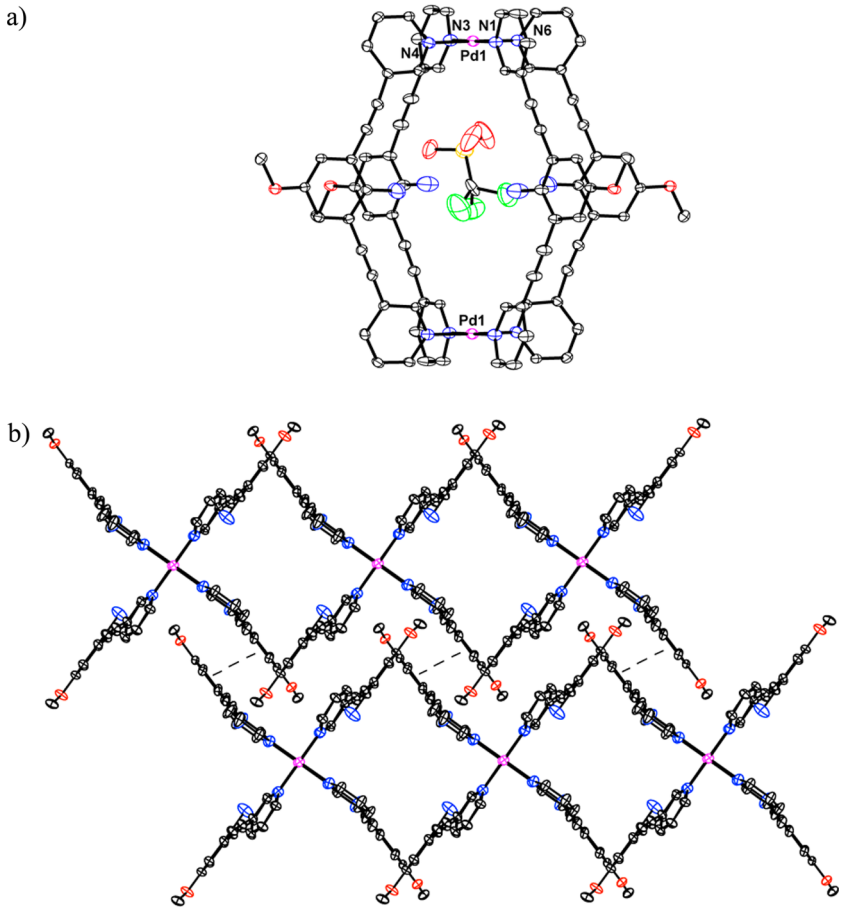

Figure 4. (a) X-ray crystal structure of the cationic part of [**3**][OTf]$_3$·5CH$_3$CN showing the triflate anion within the cavity. Color code: C, black; O, red; N, blue; Pd, violet. Hydrogen atoms and solvent molecules are omitted for clarity. Selected bond lengths (Å) and angles (deg): Pd1−Pd1 11.812(2), Pd−N1 2.012(2), Pd1−N4 2.031(2), Pd1−N3 2.028(3), Pd1−N6 2.022(3); N1−Pd1−N3 179.82, N4−Pd1−N6 178.49. (b) 2D networks of metallacapsules [**3**][OTf]$_3$·5CH$_3$CN generated by $\pi-\pi$ contacts among individual units.

for the structures reported in this paper have been deposited at the Cambridge Crystallographic Data Centre as CCDC 949856 (**3**) and 949857 (**4**). These data can be obtained free of charge from the Cambridge Crystallographic Data Centre via www.ccdc.cam.ac.uk. See the Supporting Information (SI).

Crystal Data for [3][OTf]$_3$·5CH$_3$CN: yellow crystals, $C_{98}H_{75}F_{12}N_{17}O_{16}Pd_2S_4$, triclinic, $P\bar{1}$, a = 13.0241(12) Å, b = 13.3619(14) Å, c = 17.873(3) Å, α = 98.136(7)°, β = 97.312(7)°, γ = 109.328(5)°, V = 2854.6(6) Å^3, Z = 1, T = 200(1) K, μ = 0.473 mm^{-1}, 71465 reflections measured, 18246 independent (R_{int} =

dx.doi.org/10.1021/ic402539x | Inorg. Chem. 2014, 53, 4287−4294

0.0414), 14624 observed [$I > 2\sigma(I)$], 674 parameters, final R indices R1 [$I > 2\sigma(I)$] = 0.0720 and wR2 (all data) = 0.2394, GOF (on F^2) = 1.077, max/min residual electron density = 2.632/−1.196 e Å^{-3}.

Crystal Data for [4][OTf]$_2$·3CH$_3$CN·2H$_2$O: yellow crystals, $C_{92}H_{73}F_6N_{19}O_{20}Pd_2PtS_2$, triclinic, $P\bar{1}$, a = 12.2300(5) Å, b = 13.5899(5) Å, c = 16.4293(7) Å, α = 90.570(2)°, β = 100.104(2)°, γ = 105.592(2)°, V = 2584.65(18) Å^3, Z = 1, T = 200(1) K, μ = 1.819 mm^{-1}, 118345 reflections measured, 15880 independent (R_{int} = 0.0212), 13465 observed [$I > 2\sigma(I)$], 780 parameters, final R indices R1 [$I > 2\sigma(I)$] = 0.0490 and wR2 (all data) = 0.1623, GOF (on F^2) = 1.140, max/min residual electron density = 1.975/−1.807 e Å^{-3}.

RESULTS AND DISCUSSION

Synthesis and Characterization of the Assembling Ligand 2. To demonstrate the viability of our strategy, we first prepared ligand **2** from 2,6-dibromo-4-methoxyaniline through a palladium/copper Sonogashira cross-coupling reaction to give the related diacetylene aniline derivative **1** (Scheme 1). A subsequent palladium/copper Sonogashira cross-coupling reaction with bromopyridine provided the assembling ligand **2** in 73% overall yield, as fully characterized by IR, NMR, mass spectrometry, and elemental analysis.[20b]

Synthesis and Characterization of Metallacages [3][OTf]$_3$ and [4][OTf]$_2$. Ligand **2** was treated with freshly prepared [Pd(CH$_3$CN)$_4$][OTf]$_2$ in an acetonitrile solution to afford the cage complex [**3**][OTf]$_3$. The tetragonal cationic cage was isolated and characterized as its triflate salt in 90% yield (Scheme 2). The X-ray molecular structure confirmed the presence of one encapsulated triflate anion (vide infra).

The IR spectrum of [**3**][OTf]$_3$ shows the presence of triflate anions at 1236 cm^{-1} and displays the alkyne stretching transition at 2205 cm^{-1}. The ESI-MS spectrum clearly indicates the formation of [Pd$_2$L$_4$] species in association with varying numbers of triflate counterions (Figure 2).

Moreover, the molecular capsule was found to be stable both in the solid state and in solution and to be soluble in common polar solvents such as acetonitrile, acetone, and methanol. The ^{1}H NMR spectrum of [**3**][OTf]$_3$ was recorded in CD$_3$CN and displayed a symmetric pattern similar to that of the ligand **2**. However, we note that upon coordination to the palladium center a downfield shift is observed for [**3**][OTf]$_3$, particularly for H$_j$, H$_k$, and the two N−H amino protons (Scheme 2 and Figure S1 in the SI).

Remarkably, the ^{19}F NMR spectrum of [**3**][OTf]$_3$ recorded at room temperature in acetone-d_6 showed two singlets in a roughly 3:1 intensity ratio: a singlet at −78.7 ppm attributed to free triflate anions and a weaker, broad signal at −75.8 ppm, which we assign to the encapsulated anion (Figure 3). This result confirms the presence of a triflate anion inside the cavity in solution slowly exchanging on the NMR time scale and corroborates the findings obtained by X-ray crystallography (vide infra).[21]

X-ray Molecular Structure of [3][OTf]$_3$. To ascertain the molecular structure of [**3**][OTf]$_3$, an X-ray structural determination was carried out. Crystals were grown by vapor diffusion of diethyl ether into a solution of the complex in CH$_3$CN. The molecular cage [**3**][OTf]$_3$ crystallized as 5CH$_3$CN solvate in the triclinic space group $P\bar{1}$. The structure shows the formation of a tetragonal cage, where each palladium adopts a square-planar geometry as a result of coordination to four pyridine arms of the bridging ligands **2** (Figure 4a). The Pd−N bond distances lie in the range of 2.012−2.030(3) Å and are comparable to those reported for related palladium cages.[4a,f,20] The Pd−Pd distance is 11.892(2) Å and the average distance between two facing phenyl rings is 9.502(2) Å. Furthermore, one triflate anion is present inside the cage cavity through a weak hydrogen-bonding interaction with the amine groups, while the three other anions are disordered and located outside the cavity. Of interest, we note further $\pi-\pi$ interactions between the central ring and the acetylene groups of two M$_2$L$_4$ neighbors to generate a 2D network constituted of 3D capsules and in a manner similar to that reported by Hooley and co-workers[20a] for a metallacage with endohedral amine groups (Figure 4b). It is well established that noncovalent $\pi-\pi$ interactions maintain the coherence of coordination assemblies with different geometrical forms and influence their properties.[20c,d]

On the other hand, the presence of an encapsulated anion inside the cavity led us to investigate the host−guest properties of this metallacage with endohedral amine groups using more challenging guest molecules.

We reasoned that recognition could be enhanced through synergetic interactions (mainly hydrogen bonding) provided by the amine groups pointing toward the interior of the cavity and electrostatic interactions of the positively charged palladium(II) cations. Thus, the metal complex guest [Pt(NO$_2$)$_4$]$^{2-}$ was chosen. Only a few examples are known where a square metal complex is encapsulated within a metallacage.[10−13]

Indeed, when the metallacage compound [**3**][OTf]$_3$ was titrated with 1 equiv of K$_2$[Pt(NO$_2$)$_4$] in DMSO-d_6, immediate and significant shifts were observed in the ^{1}H NMR spectrum, which suggested the formation of a novel complex of stoichiometry {[Pt(NO$_2$)$_4$]⊂[Pd$_2$(**2**)$_4$][OTf]$_2$} ([**4**][OTf]$_2$; Figure S2 in the SI). For instance, the signals attributed to hydrogen atoms H$_j$ and H$_k$ moved from 9.45 and 9.23 ppm in the metallacage [**3**][OTf]$_3$ to 9.32 and 9.22 ppm in [**4**][OTf]$_2$. Moreover, no changes in the ^{1}H NMR spectrum of [**4**][OTf]$_2$ occurred upon allowing the solution to stand over time, suggesting that this host−guest system is kinetically and thermodynamically stable.

To confirm the formation of the host−guest system [**4**][OTf]$_2$, the reaction was repeated in CH$_3$CN, and an orange precipitate was then isolated and fully characterized as [**4**][OTf]$_2$. The IR spectra showed the triflate anion bands at 1235 cm^{-1} and the alkyne and nitro group stretching bands at 2201 cm^{-1} and 1311 and 1331 cm^{-1}, respectively. The existence of the assembly [**4**][OTf]$_2$ in solution was corroborated by ESI-MS. The 2+ charge state of the {[Pt(NO$_2$)$_4$]⊂[Pd$_2$(**2**)$_4$]} fragment appears at m/z 946.12 and was verified by a comparison of the observed and theoretical isotopic patterns (Figure 5).

X-ray Molecular Structure of [4][OTf]$_2$. Gratifyingly, using slow vapor diffusion of diethyl ether into an acetonitrile/DMF (1:2) solution of [**4**][OTf]$_2$, we were successful in growing single crystals suitable for X-ray crystal structure determination. The molecular cage [**4**][OTf]$_2$ crystallized with three molecules of CH$_3$CN and two molecules of H$_2$O. As expected from the solution experiments, all M$_2$L$_4$ cages were found to contain one molecule of the anionic square-planar [Pt(NO$_2$)$_4$]$^{2-}$ complex (Figure 6).

The Pd−N bond lengths lie in the range of 2.073(1)−2.034(1) Å, very close to that observed in the previous cage [**3**][OTf]$_3$. The Pd−Pd distance is 11.417(1) Å, slightly smaller than that of [**3**][OTf]$_3$. Moreover, unlike [**3**][OTf]$_3$, the distances between adjacent facing phenyl rings are non-equivalent and lie in the range of 8.573(1)−10.815(1) Å, which average to 9.694(1) Å. This might be due to the nature

dx.doi.org/10.1021/ic402539x | Inorg. Chem. 2014, 53, 4287−4294

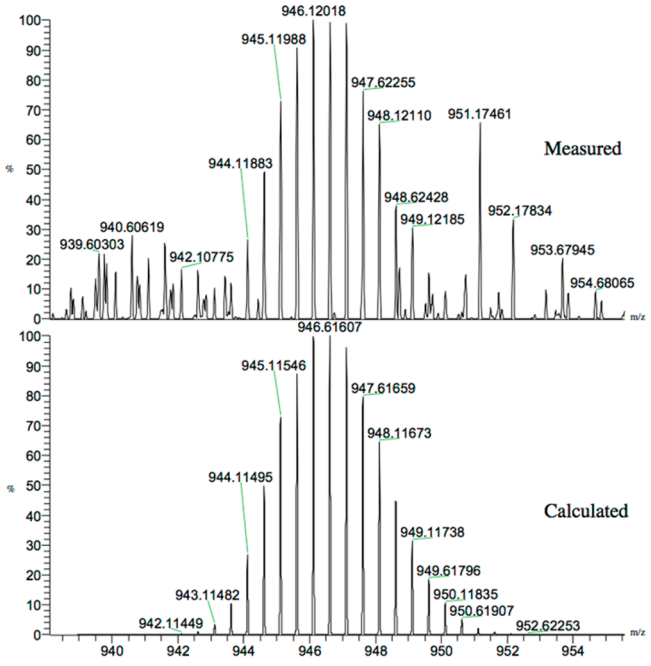

Figure 5. Calculated and observed isotope patterns for the intact metallacage $\{[Pt(NO_2)_4]\subset[Pd_2(\mathbf{2})_4]^{2+}$ (**4**).

and size of the encapsulated square-planar metal guest. Furthermore, the structure revealed the presence of two molecules, **4a** and **4b**, in the unit cell in a 6:4 ratio. These correspond to two different orientations adopted by the anionic complex guest within the cavity, determined by the nature of the host–guest interactions. For instance, in molecule **4a** (Figure 6a), $[Pt(NO_2)_4]^{2-}$ is located in the center of the cavity. Each palladium center of the cage binds to the platinum complex through a metal–oxygen coordination bond of the NO_2 moiety with a Pd–O bond distance of 2.964 Å. Interestingly, the two other NO_2 units of the anionic guest interact within the frame of the cage via hydrogen bonding to the amino functions $-NH_2$ (as hydrogen donor sites), while the $-NO_2$ oxygen atoms act as hydrogen acceptor sites. As shown in Figure 6a, the hydrogen-bonding interactions with the encapsulated guest involve the four endohedral amines. In molecule **4b**, two Pd–O interactions were also detected involving $-NO_2$ oxygen atoms, with a Pd–O bond distance of 2.964 Å, as found in molecule **4a**. However, stronger hydrogen-bonding interactions were observed between the two $-NH_2$ groups of the cage and the two $-NO_2$ oxygen atoms of the guest. We note, in this case, that two of the capsule's amino groups are not engaged in the formation of hydrogen bonds with the encapsulated guest (Figure 6b).

Density Functional Theory (DFT) Calculations on the Host–Guest System [4][OTf]$_2$. To shed light on the nature of the host–guest interactions within $[\mathbf{4a}][OTf]_2$ and $[\mathbf{4b}][OTf]_2$, DFT calculations were carried out. Geometry optimizations and natural bond order analyses were carried out on the two observed configurations by means of B3LYP theory,[22a,b] using a cc-pVDZ basis set[22c] for the main-group atoms and CEP-121G[22d] for the transition metals. Using the structures determined by X-ray diffraction (XRD) as initial geometries, the optimizations converged to structures qualitatively consistent with the two observed forms, **4a** and **4b**.

Gross features of the host cavity are well-predicted by DFT calculations. In **4a**, for example, the Pd–Pd separation of 11.5 Å determined by XRD is predicted at 11.7 Å, and the calculated and measured separations between amino nitrogen atoms on opposite sides of the Pd–Pt–Pd axis agree to within 0.1 Å. For **4b**, the macrocycle in XRD is more asymmetric than that in the calculated structure, and one of the observed amino N–N distances is larger by nearly 0.5 Å than the calculated value, whereas the Pd–Pd distance and the other N–N distance from experiment and from calculation agree to within 0.1 Å.

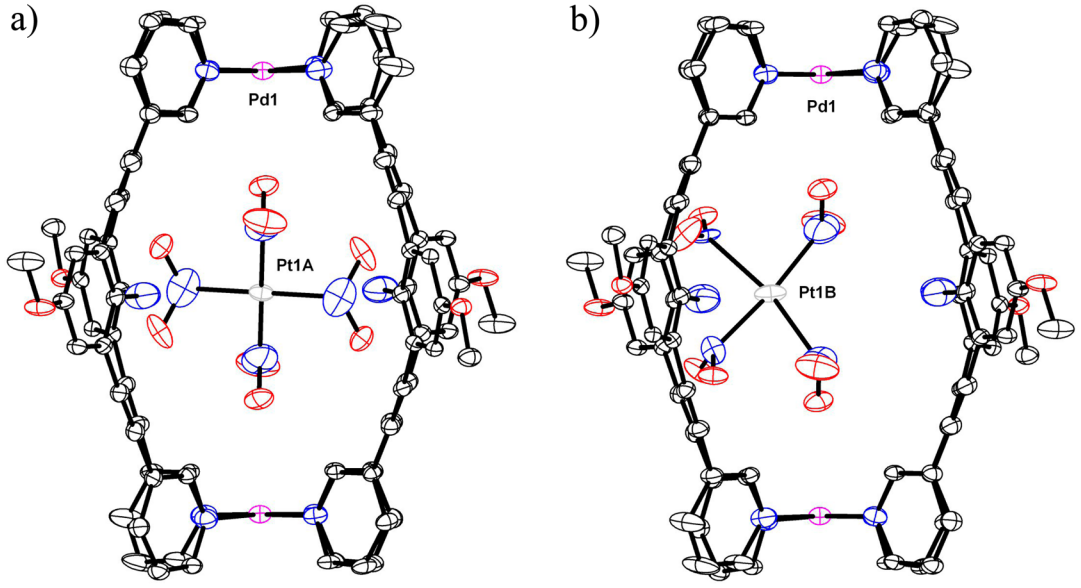

Figure 6. X-ray molecular structure of $[\mathbf{4}][OTf]_2\cdot 3CH_3CN\cdot 2H_2O$ showing the encapsulated metal complex $[Pt(NO_2)_4]^{2-}$ displaying two different orientations in molecules **4a** and **4b**. Color code: C, black; O, red; N, blue; Pd, violet; Pt, gray. Hydrogen atoms and solvent molecules are omitted for clarity. Selected bond lengths (Å) and angles (deg): Pd1–Pd1 11.417(1), Pd–N1 2.027(1), Pd1–N4 2.030(1), Pd1–N3 2.034(1), Pd1–N6 2.027(1); N1–Pd1–N3 179.82, N4–Pd1–N6 178.49. (a) Molecule **4a**: Pt1A–N7 1.8816(1), Pt1A–N8A 1.9992(1), Pd1–O3 2.964. (b) Molecule **4b**: Pt1B–N7 2.248(1), Pt1B–N8B 2.241(1), Pt1B–N9B 2.089(1), Pd1–O3 2.964.

dx.doi.org/10.1021/ic402539x | Inorg. Chem. 2014, 53, 4287–4294

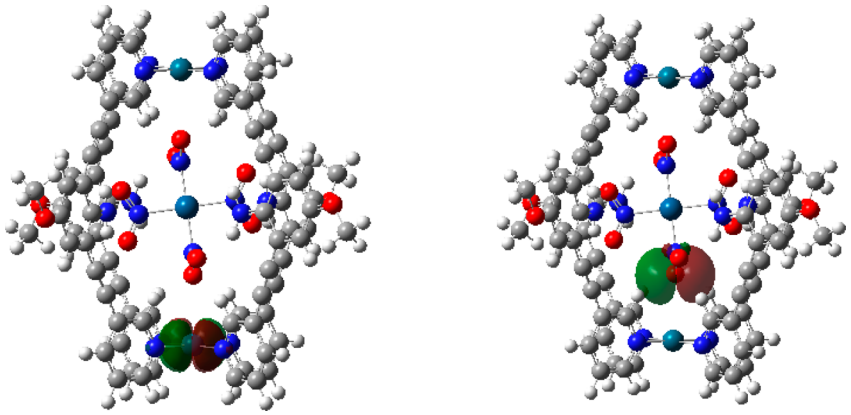

Figure 7. Representative oxygen atom lone pair and unoccupied Pd d orbitals in **4a**. Color code: O, red; N, blue; C, gray; Pd and Pt, blue-green.

While the XRD and DFT geometries of the cage itself agree well, the calculated large-scale geometries of the isolated (effectively gas-phase) species differ perceptibly from the structure determined by X-ray in the crystal. The largest of these differences are roughly 10° deviations in the dihedral angles formed by the planes of the two macrocycles that form the cage. However, as these differences do not appear to greatly impact the solvent cage geometry otherwise, we expect this gas-phase model to still serve as an adequate model of the host–guest interactions.

The relative energies of **4a** and **4b** are correctly predicted to be similar, but with **4b** more stable than **4a** by 4.8 kcal/mol, the observed relative abundances indicate that **4a** should be slightly more stable than **4b**. Because the calculations neglect lattice effects and vibrational corrections, an error in the calculated relative energy of some 5 kcal/mol is not surprising.

For both configurations, at least two distinct binding mechanisms are available to anchor the guest nitro groups: (i) complexation to the host palladium atoms and (ii) hydrogen bonding to the host amino groups. The geometries indicate that **4a** and **4b** may each take advantage of both mechanisms but to varying degrees. In the DFT structures, **4a** aligns one N–Pt–N axis at an angle of just 19° from the Pd–Pt–Pd axis, attaining the minimum possible separation of 3.0 Å between two of the nitro oxygen atoms and the neighboring palladium atoms. The other two nitro groups are positioned with their oxygen atoms at 2.1–2.2 Å from amino group hydrogen atoms, to be stabilized by hydrogen bonding. In **4b**, the guest is rotated to give 45° angles of the N–Pt–N axes with respect to the Pd–Pt–Pd axis. This positions the nitro groups so that six of the eight oxygen atoms lie 2.0–2.3 Å from an amino hydrogen atom. The remaining two oxygen atoms are part of a nitro group, which has been twisted 90° to take advantage of oxygen atom complexation to the palladium atom rather than the available hydrogen bonding to the amino groups.

In summary, form **4a** relies primarily on oxygen–metal complexation for host–guest binding, whereas form **4b** relies primarily on hydrogen bonding. The orbital analysis of both configurations find the energy differences between the lowest unoccupied Pd d orbital and the highest occupied lone-pair orbital on the neighboring oxygen to be only 8—11 kcal/mol, consistent with favorable complexation. Two of the relevant orbitals for form **4a** are shown in Figure 7.

CONCLUSION

In conclusion, we have reported a member of a novel class of palladium-based nanocages. This nanocage displayed two complementary effects that operate in synergy for the encapsulation of a kinetically labile metal complex, $[Pt(NO_2)_4]^{2-}$. Single-crystal XRD measurements show that the guest adopts two different orientations depending on the nature of the host–guest interactions involved. DFT calculations support our conclusions regarding the nature of the host–guest interactions. These studies pave the way to a better comprehension of chemical interaction and transformation within confined nanospaces.

ASSOCIATED CONTENT

Supporting Information

Detailed information in CIF format on the crystal structures of $[\mathbf{3}][OTf]_3$ and $[\mathbf{4}][OTf]_2$, NMR spectra titration data (Figures S1–S3), and DFT calculations (Tables S1 and S2). This material is available free of charge via the Internet at http://pubs.acs.org.

AUTHOR INFORMATION

Corresponding Authors

*E-mail: christophe.desmarets@upmc.fr.
*E-mail: hani.amouri@upmc.fr.

Notes

The authors declare no competing financial interest.

ACKNOWLEDGMENTS

We thank CNRS and UPMC for supporting this work. A.L.C. thanks the NSF for equipment support.

REFERENCES

(1) (a) Lehn, J.-M. *Supramolecular Chemistry, Concept and Perspectives*; VCH: Weinheim, Germany, 1995. (b) Steed, J. W.; Atwood, J. L. *Supramolecular Chemistry*; Wiley: Chichester, U.K., 2000.

(2) (a) Amouri, H.; Desmarets, C.; Moussa, J. *Chem. Rev.* **2012**, *112*, 2015. (b) Chakrabarty, R.; Mukherjee, P. S.; Stang, P. J. *Chem. Rev.* **2011**, *111*, 6810. (c) Ward, M. D. *Chem. Commun.* **2009**, 4487. (d) Smulders, M. M. J.; Riddell, I. A.; Browne, C.; Nitschke, J. R. *Chem. Soc. Rev.* **2013**, *42*, 1728.

(3) (a) Caulder, D. L.; Raymond, K. N. *Acc. Chem. Res.* **1999**, *32*, 975. (b) Albrecht, M. *Chem. Rev.* **2001**, *101*, 3457. (c) Xu, J.; Raymond, K. N. *Angew. Chem., Int. Ed.* **2006**, *45*, 6480. (d) Albrecht, M.; Frohlich, R. *Bull. Chem. Soc. Jpn.* **2007**, *80*, 797.

(4) (a) Freye, S.; Michel, R.; Stalke, D.; Pawliczek, M.; Frauendorf, H.; Clever, G. H. *J. Am. Chem. Soc.* **2013**, *135*, 8476. (b) Johnstone, M.

D.; Frank, M.; Clever, G. H.; Pfeffer, F. M. *Eur. J. Org. Chem.* **2013**, 5848. (c) Kopilevich, S.; Gil, A.; Garcia-Ratés, M.; Bonet-Ávalos, J.; Bo, C.; Müller, A.; Weinstock, I. A. *J. Am. Chem. Soc.* **2012**, *134*, 13082. (d) Bivaud, S.; Balandier, J.-Y.; Chas, M.; Allain, M.; Goeb, S.; Sallé, M. *J. Am. Chem. Soc.* **2012**, *134*, 11968. (e) Scott, S. O.; Gavey, E. L.; Lind, S. J.; Gordon, K. C.; Crowley, J. D. *Dalton Trans.* **2011**, *40*, 12117. (f) Mirtschin, S.; Slabon-Turski, A.; Scopelliti, R.; Velders, A. H.; Severin, K. *J. Am. Chem. Soc.* **2010**, *132*, 14004. (g) Han, Y.-F.; Jia, W.-G.; Yu, W.-B.; Jin, G.-X. *Chem. Soc. Rev.* **2009**, *38*, 3419. (h) Li, Z.; Kishi, N.; Hasegawa, K.; Akita, M.; Yoshizawa, M. *Chem. Commun.* **2011**, *47*, 8605. (i) Kishi, N.; Li, Z.; Yoza, K.; Akita, M.; Yoshizawa, M. *J. Am. Chem. Soc.* **2011**, *133*, 11438. (j) Freudenreich, J.; Dalvit, C.; Süss-Fink, G.; Therrien, B. *Organometallics* **2013**, *32*, 3018. (k) Desmarets, C.; Ducarre, T.; Rager, M. N.; Gontard, G.; Amouri, H. *Materials* **2014**, *7*, 287.

(5) (a) Amouri, H.; Rager, M. N.; Cagnol, F.; Vaissermann, J. *Angew. Chem., Int. Ed.* **2001**, *40*, 3636. (b) Saalfrank, R. W.; Dresel, A.; Seitz, V.; Trummer, S.; Hampel, F.; Teichert, M.; Stalke, D.; Stadler, C.; Daub, J.; Schunemann, V.; Trautwein, A. X. *Chem.—Eur. J.* **1997**, *3*, 2058.

(6) (a) Su, C.-Y.; Cai, Y.-P.; Chen, C.-L.; Smith, M. D.; Kaim, W.; zur Loye, H.-C. *J. Am. Chem. Soc.* **2003**, *125*, 8595. (b) Mimassi, L.; Guyard-Duhayon, C.; Rager, M. N.; Amouri, H. *Inorg. Chem.* **2004**, *43*, 6644. (c) Mimassi, L.; Cordier, C.; Guyard-Duhayon, C.; Mann, B. E.; Amouri, H. *Organometallics* **2007**, *26*, 860. (d) Therrien, B. *Eur. J. Inorg. Chem.* **2009**, 2445. (e) Schmitt, F.; Freudenreich, J.; Barry, N. P. E.; Juillerat-Jeanneret, L.; Süss-Fink, G.; Therrien, B. *J. Am. Chem. Soc.* **2012**, *134*, 754.

(7) Raehm, L.; Mimassi, L.; Guyard-Duhayon, C.; Amouri, H.; Rager, M. N. *Inorg. Chem.* **2003**, *42*, 5654.

(8) (a) Bivaud, S.; Goeb, S.; Croué, V.; Dron, P. I.; Allain, M.; Sallé, M. *J. Am. Chem. Soc.* **2013**, *135*, 10018. (b) Therrien, B. *Chem.—Eur. J.* **2013**, *19*, 8378 and references cited therein.

(9) (a) Amouri, H.; Mimassi, L.; Rager, M. N.; Mann, B. E.; Guyard-Duhayon, C.; Raehm, L. *Angew. Chem., Int. Ed.* **2005**, *44*, 4543. (b) Amouri, H.; Desmarets, C.; Bettoschi, A.; Rager, M. N.; Boubekeur, K.; Rabu, P.; Drillon, M. *Chem.—Eur. J.* **2007**, *13*, 5401. (c) Desmarets, C.; Poli, F.; Le Goff, X. F.; Muller, K.; Amouri, H. *Dalton Trans.* **2009**, 10429.

(10) (a) Yoshizawa, M.; Ono, K.; Kumazawa, K.; Kato, T.; Fujita, M. *J. Am. Chem. Soc.* **2005**, *127*, 10800. (b) Ono, K.; Yoshizawa, M.; Kato, T.; Fujita, M. *Chem. Commun.* **2008**, 2328. (c) Ono, K.; Yoshizawa, M.; Akita, M.; Kato, T.; Tsunobuchi, Y.; Ohkoshi, S.; Fujita, M. *J. Am. Chem. Soc.* **2009**, *131*, 2782.

(11) Therrien, B.; Süss-Fink, G.; Govindaswamy, P.; Renfrew, A. K.; Dyson, P. J. *Angew. Chem., Int. Ed.* **2008**, *47*, 3773.

(12) Clever, G. H.; Kawamura, W.; Tashiro, S.; Shiro, M.; Shionoya, M. *Angew. Chem., Int. Ed.* **2012**, *51*, 2606.

(13) Lewis, J. E. M.; Gavey, E. L.; Cameron, S. A.; Crowley, J. D. *Chem. Sci.* **2012**, *3*, 778.

(14) Popeney, C.; Guan, Z. *Organometallics* **2005**, *24*, 1145.

(15) Drent, E.; Van Broekhoven, J. A. M.; Doyle, M. J. *J. Organomet. Chem.* **1991**, *417*, 235.

(16) Blessing, R. H. *Acta Crystallogr.* **1995**, *A51*, 33.

(17) Altomare, A.; Cascarano, G.; Giacovazzo, C.; Guagliardi, A. *J. Appl. Crystallogr.* **1993**, *26*, 343.

(18) Palatinus, L.; Chapuis, G. *J. Appl. Crystallogr.* **2007**, *40*, 786.

(19) Sheldrick, G. M. *Acta Crystallogr., Sect. A* **2008**, *64*, 112.

(20) (a) Johnson, A. M.; Moshe, O.; Gamboa, A. S.; Langloss, B. W.; Limtiaco, J. F. K.; Larive, C. K.; Hooley, R. J. *Inorg. Chem.* **2011**, *50*, 943. (b) Pollock, B.; Cook, T. R.; Stang, P. J. *J. Am. Chem. Soc.* **2012**, *134*, 10607. (c) Amouri, H.; Caspar, R.; Gruselle, M.; Guyard-Duhayon, C.; Boubekeur, K.; Lev, D. A.; Collins, L. S. B.; Grotjahn, D. B. *Organometallics* **2004**, *23*, 4338. (d) Moussa, J.; Wong, K. M.-C.; Le Goff, X. F.; Rager, M. N.; Chan, C. K.-M.; Yam, V. W.-W.; Amouri, H. *Organometallics* **2013**, *32*, 4985.

(21) We thank a reviewer for suggesting the ^{19}F NMR experiment.

(22) (a) Becke, A. D. *J. Chem. Phys.* **1993**, *98*, 5648. (b) Lee, C.; Yang, W.; Parr, R. G. *Phys. Rev. B* **1988**, *37*, 785. (c) Dunning, J. T. H. *J. Chem. Phys.* **1989**, *90*, 1007. (d) Stevens, W. J.; Krauss, M.; Basch, H.; Jasien, P. G. *Can. J. Chem.* **1992**, *70*, 612.

NOTE ADDED AFTER ASAP PUBLICATION

This paper was published on the Web on April 11, 2014, with the incorrect Synopsis text. The corrected version was reposted on April 15, 2014.